



Experimental study on fractal characteristics of seepage-induced failure in granular soil

Yu Wang¹ · Yanchen Liu¹ · Buxiang Wang²

Received: 9 March 2023 / Revised: 17 March 2023 / Accepted: 13 June 2023 / Published online: 30 June 2023
© The Author(s) under exclusive licence to OWZ 2023

Abstract

Seepage-induced failures in granular soils pose a potential hazard for geotechnical engineering, but the types and mechanisms of seepage failures have not been fully clarified. In this paper, the mass fractal dimensions of testing soils were used to describe the cumulative mass distribution of particles, which was closely related to the uniformity coefficient, fine content, porosity, dry density and permeability coefficient. A series of hydraulic tests were performed to show seepage failure behaviors of sandy gravels, coarse sands and fine sands. By linking the mass fractal dimension to the critical hydraulic gradient, a zone segmentation approach for seepage failure types was proposed to distinguish seepage failures, including piping, suffosion and heave. Piping failure originates from internal instabilities in inhomogeneous soils and has been observed in sandy gravel samples. Suffosion occurs in coarse sand samples due to external and internal erosion of loose particles. Heave failure is dominated by fine content and has been observed in fine sand samples. By comparing the changes in the mass fractal dimension before and after seepage failure, it is feasible to predict piping failure in sandy gravels and suffosion in loose coarse sands, while it is almost impossible to predict heave failure in fine sands.

Keywords Fractal · Seepage failure · Particle migration · Granular soil · Piping

List of symbols

C	Constant (–)
C_u	Uniformity coefficient (–)
D	Arbitrary particle size (L)
D_m	Mass fractal dimension (–)
d_{10}	Particle size for which 10% are smaller (L)
d_{60}	Particle size for which 60% are smaller (L)
F	Fines percent corresponding to an arbitrary particle diameter D (–)
H	Difference of the fines percent between D and $4D$ (–)
i_{cr}	Critical hydraulic gradient (–)
K	Permeability coefficient (LT^{-1})
K_s	Slope (–)
M_T	Total mass (M)

n	Porosity (–)
P_f	Fine content (–)
R	Correlation coefficient (–)
r	Sieve size opening (L)
r_L	Maximum particle size (L)
ρ_d	Dry density (MT^{-3})

1 Introduction

Seepage-induced failure in granular soil can lead to serious disasters such as groundwater contamination, foundation collapse and dam breach. Granular soil, as the main material of dam bodies, foundations and filters, is more likely to trigger seepage failure due to the loss of the integrity of the soil caused by seepage flows [1]. Given the complexity of water–soil interactions, seepage failure shows various types in which the development mechanisms are quite different [2]. A clear distinction of seepage failures in granular soils should be drawn to reduce the risk of potential disasters and guarantee the long-term safety of hydraulic engineering operations.

Yu Wang and Yanchen Liu were contributed equally to this work.

✉ Yu Wang
wangyu@jsou.edu.cn

¹ College of Civil Engineering, Jiangsu Open University, Nanjing 210036, China

² Huatian Engineering and Technology Corporation, Nanjing 210000, China

Seepage failure takes different forms, including backward erosion piping, concentrated leak erosion, contact erosion, and suffusion [3]. Backward erosion piping indicates that the surface particles are detached from the downstream exit along the direction of the percolation flow [4]. Concentrated leak erosion occurs mostly in cohesive soils, where the seepage path resembles a crack [5]. Contact erosion indicates erosion of the fine soil by seepage through the interface between the coarse soil and the fine soil, or between the soil and other materials, e.g., the contact surface of the concrete conduit throughout the dam [6]. Suffusion describes the motion of finer particles through the voids of coarser particles with non-destructive volume deformation, leaving the coarser skeleton intact [7, 8]. While the term “suffusion” is considered to describe the internal instability with a reduction in the volume of the soil [9, 10]. Whatever form it takes, seepage failure occurs once internal erosion has progressed to a certain point at a critical hydraulic gradient [11, 12]. In this study, seepage failures are those which may cause a deformation of the soil structure, accompanied by the phenomena observed in hydraulic tests of piping, heave, or suffusion.

Seepage-induced failure depends on the intrinsic conditions of soil internal stability and hydraulic conditions. The earliest method for assessing the hydraulic conditions of the heave of sand was proposed by Terzaghi, who compared the vertical hydraulic gradient with the critical hydraulic gradient required to trigger erosion [13]. The critical hydraulic gradient can be obtained by either a hydraulic test or an empirical formula. However, soil internal stability can be evaluated by the particle size distribution (PSD) or the constriction size distribution (CSD) [14, 15]. On this basis, different criteria were suggested to evaluate potential seepage failure [16]. The uniformity coefficient C_u (d_{60}/d_{10}) and fine content P_f obtained from PSD are important parameters for the distinction of seepage failure types. For example, heave failure or flow soil, described in Chinese hydraulic and geotechnical literatures, may occur in granular soil if $C_u \leq 5$ or the conditions of $C_u > 5$ and $P_f > 35\%$ are both satisfied, while piping failure is more likely to occur when the conditions of $C_u > 5$ and $P_f < 25\%$ are met. If the conditions of $C_u > 5$ and $25\% \leq P_f \leq 35\%$ are satisfied, the occurrence of heave or piping failure depends on the soil gradation, particle shape and dry density, etc. [4, 17]. In addition, some studies have verified that the potential for seepage failure is largely governed by the shape of the PSD curve, and numerous geometrical criteria have been established. A method was proposed to evaluate the internal stability of granular soils experimentally [18]. The method assumes that an arbitrary particle size D could erode via a constriction formed by particle size $4D$ or larger. The value H can be easily figured out as the difference of the fines percent between D and $4D$ by determining the fines percent F corresponding to an arbitrary particle diameter D . The minimum ratio $(H/F)_{\min} < 1$ is deemed internally

unstable, presenting the characteristics of piping failure in granular soil. This criterion was validated by large experimental datasets with a high success rate [19]. For example, a combined particle and constriction size distribution approach were suggested to demarcate a clear boundary between internally stable and unstable soils through the evaluation of PSD of finer fraction and CSD of coarse fraction in tandem. Interestingly, all the criteria were unified in a single method to indicate the risk of internal instability by using a measure of the slope of the PSD curve [20].

Inspired by the above approach, the fractal dimension derived from the slope of the PSD curve may be able to describe the internal stability in self-similar soils [13, 21]. A self-similar soil is one in which a part of the whole continually resembles the whole, sometimes only in a statistical sense. Granular soils can be divided into a number of morphologically similar entities and further subdivided into morphologically similar entities [22]. The fractal nature of granular soils typically arises from fragmentation processes, including explosive disruption, impact fragmentation, weathering, and crushing [23]. Moreover, particle and pore size distributions of soils have been shown to be fractal. Seepage should also be fractal in filled spaces formed by soil particles and pore networks [24]. A fractal model of soil water retention was created to show that the fractal dimension of pore channels follows an exponential relation as a function of particle size. Unlike soil fragmentation, the seepage failure process has fractal features due to the transport of fine particles from the pore channels [21, 25]. Specifically, fine particles can be progressively washed out of the pore channel at a certain hydraulic gradient, resulting in an increase in the pore size and permeability coefficient [26]. As the hydraulic gradient continues to increase, the constant removal of fine particles induced by the seepage flow again increases the porosity of the granular soil. Subsequently, larger loose particles are carried away from the progressively extended percolation channel, which may eventually lead to seepage failure.

Although seepage failures associated with internal stability have been investigated, a method for considering both the characteristics of soil structures and hydraulic conditions to distinguish seepage failures has not yet been clarified. In addition, various development mechanisms deserve more attention due to the different types of seepage failures. The objectives of this study were to: (1) clarify the migration characteristics of particle soils and the behaviors of various seepage failures, and (2) propose a fractal method for distinguishing seepage failures to further reveal the development mechanisms.

Table 1 Physical property parameters of experimental soils

Sample number	Soil type	Uniformity coefficient C_u	Porosity n	Dry density ρ_d (g/cm^3)	Permeability coefficient K (cm/s)	Fine content P_f (%)
1	Sandy gravel	85	0.26	2.04	$3.35\text{E}-02$	28
2		91	0.25	2.16	$3.20\text{E}-02$	30
3		80	0.27	2.01	$3.50\text{E}-02$	23
4		115	0.23	2.28	$2.80\text{E}-02$	34
5		60	0.28	1.98	$4.20\text{E}-02$	18
6		40	0.30	1.95	$4.80\text{E}-02$	14
7	Coarse sand	5	0.18	1.85	$6.40\text{E}-03$	68
8		12	0.19	1.82	$8.60\text{E}-03$	63
9		20	0.20	1.78	$9.18\text{E}-03$	58
10		30	0.22	1.76	$9.50\text{E}-03$	55
11		35	0.24	1.75	$9.80\text{E}-03$	50
12		43	0.25	1.73	$1.12\text{E}-02$	42
13	Fine sand	2	0.14	1.72	$1.80\text{E}-03$	85
14		3	0.15	1.70	$2.10\text{E}-03$	81
15		3	0.16	1.65	$2.70\text{E}-03$	75
16		7	0.18	1.62	$3.10\text{E}-03$	71
17		10	0.20	1.58	$3.40\text{E}-03$	65
18		17	0.22	1.52	$3.80\text{E}-03$	61

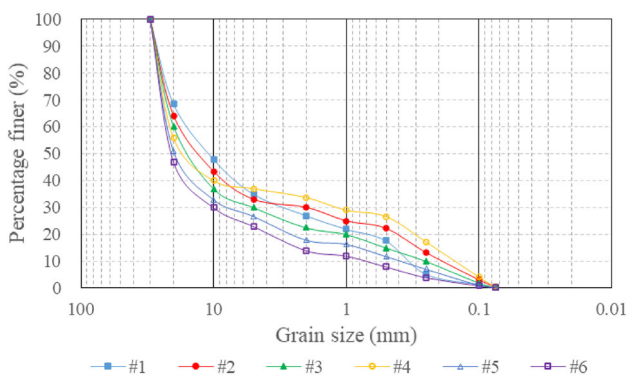


Fig. 1 Grading curve of sandy gravels numbered 1–6

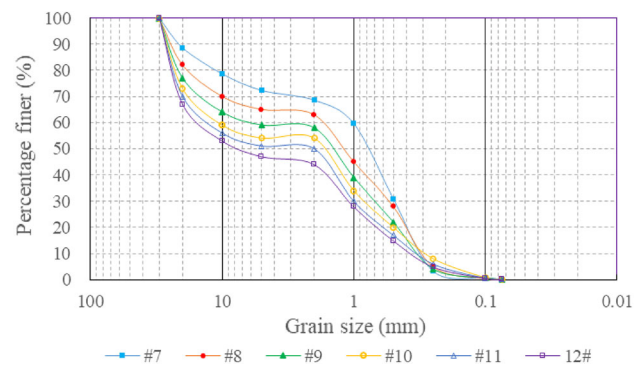


Fig. 2 Grading curve of coarse sands numbered 7–12

2 Materials and methods

2.1 Testing soils

As previously described, the mass fractal dimension is generally regarded as an inherent index to reflect the statistically self-similar characteristics related to physical and mechanical properties in granular soil. Hydraulic tests were performed to evaluate the mass fractal dimension on the seepage failure in granular soil from the banks of the Yangtze River. Granular soil samples include sandy gravels numbered 1–6 (Fig. 1), coarse-grained sands numbered 7–12 (Fig. 2),

and fine-grained sands numbered 13–18 (Fig. 3). Testing soils were prepared as follows. The cutting edge was used to press vertically into natural soils until they were filled in the ring sampler, then surrounding soils were cut off and the ring sampler was carefully taken out to keep natural soils undisturbed. Next, soil samples were divided into 9 representative grades in the light of different aperture sifters, that is, > 20 mm, 20–10 mm, 10–5 mm, 5–2 mm, 2–1 mm, 1–0.5 mm, 0.5–0.25 mm, 0.25–0.1 mm, and 0.1–0.075 mm. For the large size gravels (maximum grain diameter of 3 cm), an equivalent density method was used to keep the soil unit weight invariant by using fine particles instead of large ones. The

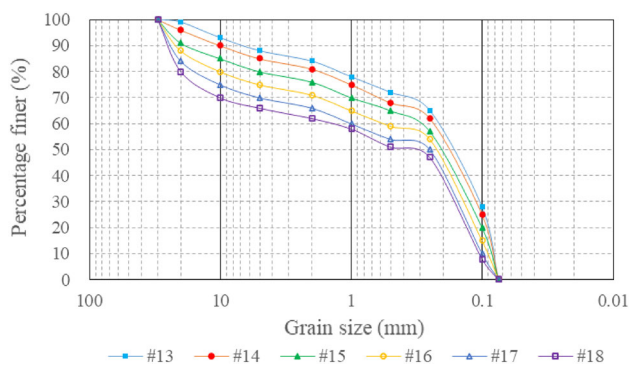


Fig. 3 Grading curve of fine sands numbered 13–18

physical property parameters of soils are presented in Table 1.

2.2 Testing apparatus

A testing apparatus was designed for granular soil to measure hydraulic pressures and gradients under the conditions of vertical seepage flow through a soil sample (Fig. 4). The general concept of the apparatus is to provide a uniform hydraulic gradient through a soil sample without converging or diverging flow conditions, thereby observing the hydraulic pressures and gradients with measuring equipment. Besides, the necessary conditions for the critical hydraulic gradient to initiate the seepage erosion process can be evaluated. A detailed description of the testing apparatus is exhibited as follows.

The apparatus consists of a water supply device, a sample holder, measuring equipment and a data collection system. The soil sample is retained in a rigid-walled Plexiglas holder sealed in a porous permeable board attached to a conical, stainless and influent water supply device. The porous permeable board at the base of the cylinder holds the soil, while allowing water to flow gradually into the soil sample. The soil sample holder is a 75.0-cm-high and 25.5-cm-diameter cylinder-shaped Plexiglas mold with two rows of pore pressure measurement ports located at the sides of the holder, which is designed to precisely measure the hydraulic pressure of seepage flow through the sample at different locations. Piezometric tubes are used to manually measure pore pressure, while sensors connected to the data collection system can automatically measure hydraulic pressure in real-time. To better improve the reliability of monitoring data, measurements are made using 9 pressure sensors (numbered a–i) installed vertically along the side of the apparatus every 5 cm, and 9 piezometric tubes (numbered 0–8) are alternately located on the opposite side every 5 cm, except for the No.0 tube, which is set in the porous permeable board to measure the upstream water head. The resulting spacing along the vertical allowed measurements every 2.5 cm to observe

minor deformation in each part of the soil in the seepage erosion process. The inside of the sample holder is coated with silicone gel that serves a dual function. First, it provides a frictional interface between the soil samples and the sample holder. Second, since porous soil sample indent into the silicon, it prevents a preferred seepage path along the edges of the sample that would occur as a consequence of larger interstitial voids caused by a lack of interlocking with the smooth Plexiglas surface.

The hydraulic pressure is flexibly governed by the water tank attached to the screw pole to produce a uniform vertical hydraulic gradient upward through a porous permeable board into the sample. The altitude adjustment is controlled by two nuts arranged on the screw pole that can be fixed on the transmission driver, and the hydraulic pressure can be slowly regulated. By controlling the upstream head of the water tank and the downstream head of the overflow mouth, the differential head across the sample is steadily increased until the initial seepage failure occurs. Both seepage behavior and soil deformation of each part of the porous soil can be observed and recorded.

2.3 Testing procedure

The testing procedure is outlined as follows:

For better control of various factors that could affect the seepage erosion, such as temperature, water content, and physical dimension of soil, the laboratory test was kept at a uniform temperature, and all soil samples were dried and prepared in a completely saturated condition, and the physical dimensions of the soil were rigidly performed.

Soils were tested with three specimen heights in the sample holder. If the content of coarse sands was high, the filling height would be large. Specifically, for sandy gravels, the filling height was 35 cm. The filling height was 30 cm for coarse-grained sands, while the filling height was 25 cm for fine-grained sands.

Two ways of water injection were used to gradually make the sample soil saturated. One was to inject water continuously to ensure that the initial hydraulic gradient was less than 0.1 and then increase to a slight hydraulic gradient increment of 0.1, which could be observed every five minutes until the hydraulic pressure on the sensors was steady or water level in piezometric tubes varied little. The other was to inject water regularly to simulate the process of the water level gradually rising, which was loaded with a tiny hydraulic gradient increment of 0.05–0.1 every 15–30 min.

The tests went on until the soil completely failed. The test was not stopped until the connected leakage pathway was formed from the bottom to the top of the soil samples or the soil particles were lifted to float in entirety. The hydraulic gradient, permeability coefficient and overflow amount were

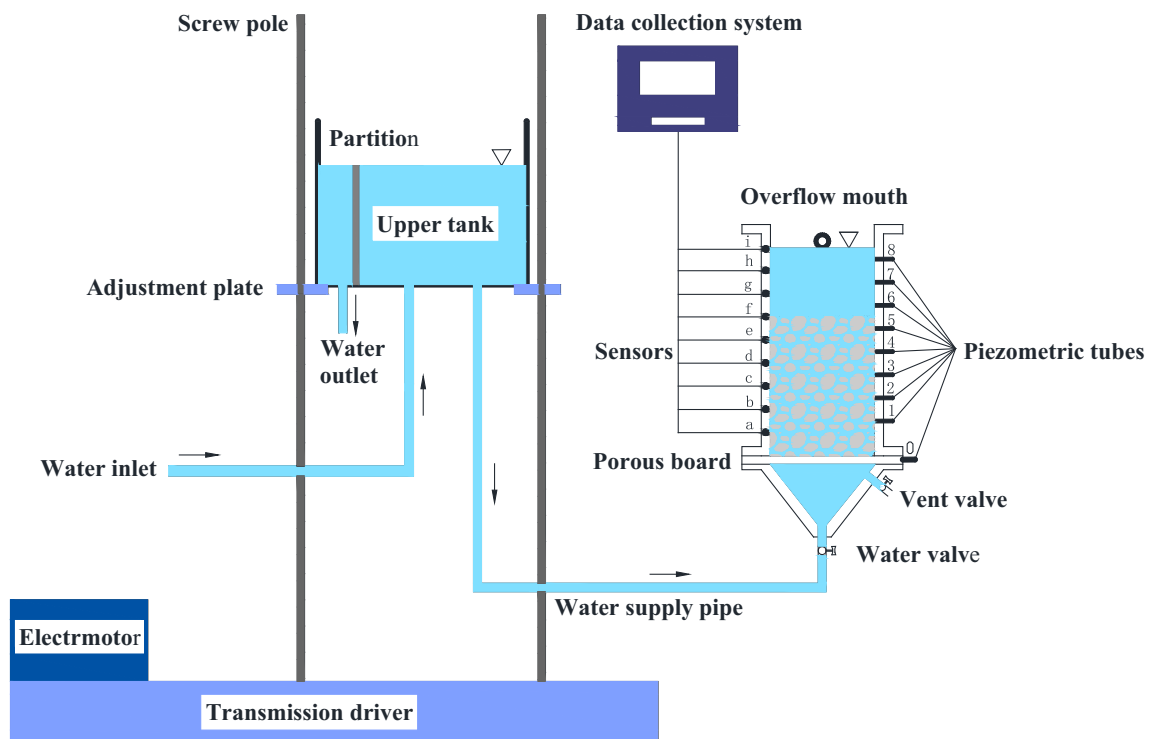


Fig. 4 Schematic illustration of testing apparatus

used as quantificational indexes. Tests ended until these parameters increased more than 10 times.

By observing the water head in the piezometric cubes, hydraulic pressure on the sensors and the opacification degree of overflow water, internal adjustments of fine particles were captured in the seepage failure process. At the same time, the hydraulic gradient and overflow amount were frequently measured to obtain adequate seepage failure data.

3 Results and discussion

3.1 Mass fractal dimension analysis

Granular soils composed of particles and pores of different sizes exhibit statistical fractal properties over a range of grain sizes. Different fractal dimensions have been proposed to quantitatively characterize the fractal properties of particle sizes and pore networks. Fractal properties of granular soils are based on the geometric fractal dimension obtained by box-counting methods or image analysis [21]. However, the statistical fractal dimension is more suitable for describing fractal features in granular soils, since scale invariance is only present in a certain range of grain sizes [22]. The mass fractal dimension, as one of the statistical fractal dimensions, is commonly used for particle mass accumulation in geoen지니어링 [27]. Moreover, the mass fractal dimension is conveniently

obtained based on the grading curve, which is relevant for the grain size distribution of granular soils. Following this concept within the study, the mass fractal dimension has been used to quantitatively describe the mass accumulation associated with the particle size distribution and the complexity of the pore network. The grading curve is typically presented as a percentage of the cumulative mass of the soil occupied by a given size fraction. The fractal relationship of the mass distribution can be expressed by [20]:

$$M(< r) \propto r^{3-D_m} \tag{1}$$

where $M(< r)$ is the mass of particles whose sizes are smaller than a given comparative size r ; D_m is the mass fractal dimension. A relation based on the results of a standard sieve analysis test was established by Taylor and Wheatcraft to compute the fractal dimension of soil. This relationship is [21]:

$$\frac{M(R < r)}{M_T} = \left(\frac{r}{r_L}\right)^{3-D_m} \tag{2}$$

where $M(R < r)$ is the cumulative mass of particles with size R smaller than a given comparative size r ; M_T is the total mass of particles; r is the sieve size opening; and r_L is the maximum particle size as defined by the largest sieve size

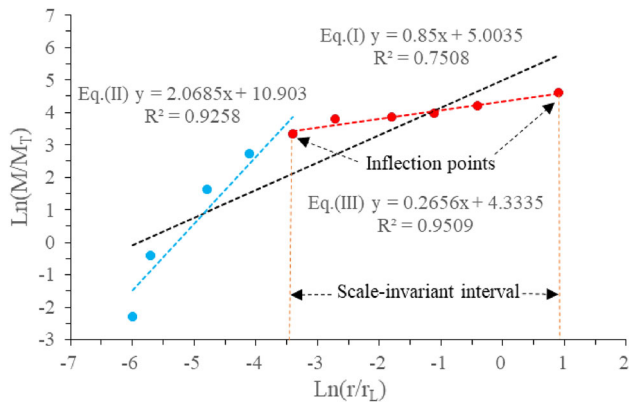


Fig. 5 The fitting curves of the mass fractal dimension calculation in a sandy gravel

opening used in the sieve analysis. Logarithmic transformations of Eq. (2) on both sides yield the following:

$$L_n \frac{M(R < r)}{M_T} = (3 - D_m)L_n \left(\frac{r}{r_L} \right) + C \tag{3}$$

where C is the constant. The fractal dimension D_m and the slope K_s of the linear fitting equation of the grading curve in $L_n M (R < r)/M_T \sim L_n (r/r_L)$ coordinates satisfy:

$$D_m = 3 - K_s \tag{4}$$

The determination of scale invariance is a precondition for an accurate calculation of the fractal dimension of the mass. Given that soil structures possess mass fractal characteristics in the range of a certain grain size, the accurate calculation of the mass fractal dimension D_m derived from the slope of the linear fitting equation needs to satisfy three necessary conditions, namely, the relevant scale-invariant interval, the reasonable fractal dimension, and the high correlation coefficient. For example, the mass fractal dimension was obtained from the fitting curve of the particle size distribution in a sandy gravel (Fig. 5). Equation (1) presents a smoothing curve fitting all the scattering points with the correlation coefficient $R^2 = 0.7508$, which means the reliability of the fitting results is poor due to the neglect of the scale range of self-similarity. Equation (2) shows that the mass fractal dimension $D_m = 3 - 2.0685 = 0.9315$ with a high correlation coefficient $R^2 = 0.9258$, but the value of the mass fractal dimension is unreasonable in light of the dimension of soils filled with various pores in space is generally between 2 and 3. In comparison, Eq. (3) shows that mass fractal dimension $D_m = 3 - 0.2656 = 2.7344$ with a high correlation coefficient $R^2 = 0.9509$, indicating that the fitting curve is relevant. This curve can be obtained by two inflection points, in the middle of which the scatter of points actually fall on a straight

line. The extent of the straight line corresponding to horizontal ordinate value reflects the range of self-similarity of the sandy gravel. The scale of the straight line corresponds to $L_n (r/r_L) = -3.5$ to 0.9 along the horizontal axis. If the largest size of particles was known and the scale-invariant interval would be immediately obtained.

The mass fractal dimensions of soil samples, including sandy gravels, coarse sands and fine sands, were determined through the fitting results of the particle grading curves. Table 2 shows the statistical results of various scale-invariant intervals and mass fractal dimensions extracted from Figs. 6, 7 and 8. The fitting curves of sandy gravels and coarse sands present double fractal characteristics, while the fitting curves of fine sands exhibit multiple fractal characteristics with a good correlation, as shown in Figs. 6, 7 and 8. Results indicate that there is a difference between the scale-invariant intervals, which may be related to the particle size distribution. The scale-invariant intervals of sandy gravels (#1–#6) range from 1 to 20 mm, while coarse sands (#7–#12) range from 0.5 to 10 mm and fine sands (#13–#18) from 0.25 to 5 mm. Furthermore, the fine content of scale-invariant largely determines the magnitude of the mass fractal dimension. For sandy gravels, the fine content of scale-invariant is between 40.11 and 79.30%, and the mass fractal dimension varies from 2.4767 to 2.7392. For coarse sands, the fine content of scale-invariant is between 81.78 and 87.21%, and the mass fractal dimension varies from 2.7344 to 2.8531. For fine sands, the fine content of scale-invariant is between 89.66 and 93.29%, and the mass fractal dimension varies from 2.8759 to 2.9234. It can be deduced that the higher the fine content of the scale-invariant interval, the larger the mass fractal dimension, which determines the physical and mechanical properties of granular soils.

3.2 Mass fractal dimension evaluation

Since the mass fractal dimension is closely related to the physical and mechanical properties of granular soil, the relationship of the mass fractal dimension to some important parameters regarding seepage failure is needed to evaluate. The uniformity coefficient (d_{60}/d_{10}) varies with the mass fractal dimension, as shown in Fig. 9. The results suggest that the uniformity coefficient of sandy gravel increases in an exponential form with the mass fractal dimension, while the uniformity coefficient of coarse sand decreases linearly and fine sand decreases in the form of approximate power law function. For sandy gravel samples, d_{60} ranges from 15 to 30 mm and d_{10} from 0.15 to 0.60 mm. With the increase of the mass fractal dimension, more fine particles occupy the skeleton pores of the soil, leading to the high degree of uniformity. For coarse sand samples, however, d_{60} ranges from 1 to 15 mm and d_{10} from 0.30 to 0.40 mm. Similarly, for fine sand samples, d_{60} ranges from 0.2 to 1 mm and d_{10} from

Table 2 Different soil samples of the mass fractal dimensions and scale-invariant intervals

Soil numbers	Soil types	Scale-invariant interval (mm)		Fine content of scale-invariant interval (%)	Mass fractal dimension	Correlation coefficient
		Lower bound	Upper bound			
1	Sandy gravel	1.00	20	58.70	2.6451	0.9660
2		1.00	20	76.92	2.6787	0.9286
3		1.00	20	55.78	2.6184	0.9488
4		1.00	20	79.30	2.7392	0.9386
5		1.00	20	51.73	2.5710	0.9461
6		1.00	20	40.11	2.4767	0.9600
7	Coarse sand	0.50	10	87.21	2.8531	0.9822
8		0.50	10	85.32	2.8349	0.9268
9		0.50	10	84.67	2.8076	0.9212
10		0.50	10	83.54	2.7817	0.9121
11		0.50	10	82.11	2.7565	0.9162
12	Fine sand	0.50	10	81.78	2.7344	0.9509
13		0.25	5	93.29	2.9234	0.9353
14		0.25	5	92.17	2.9158	0.9565
15		0.25	5	91.44	2.9064	0.9756
16		0.25	5	90.79	2.8948	0.9920
17		0.25	5	90.21	2.8822	0.9920
18		0.25	5	89.66	2.8759	0.9788

0.09 to 0.1 mm. Despite the mass fractal dimension increases further, the grain size range of $d_{60}-d_{10}$ gets smaller, which means fine particles progressively accumulate to a certain degree, greatly reducing nonuniformity of granular soil.

The content of fine particles varies with the mass fractal dimension, as shown in Fig. 10. The results suggest that the fine content P_f tends to increase linearly as the mass fractal dimension gets larger. Note that fine content P_f herein refers to soil particles with diameter < 2 mm and not < 0.075 mm, as generally assumed in the geomechanics community. For sandy gravel samples, P_f ranges from 18 to 34%, and the mass fractal dimension increases from 2.4767 to 2.7392. The mass fractal dimension is highly susceptible to the fine content accumulated in the large pores of the skeleton. For coarse sand samples, however, P_f ranges from 42 to 68%, but the mass fractal dimension only increases from 2.7344 to 2.8531, which shows that the increase of fine content is lowly susceptible to the mass fractal dimension. Obviously, the mass fractal dimension of fine sands increases less significantly because the small pores of the skeletons are only packed by finer fractions. It is verified by the fine sand samples with P_f ranging from 61 to 85%, but the mass fractal dimension simply increases from 2.8759 to 2.9234.

The porosity varies with the mass fractal dimension in soil samples, as shown in Fig. 11. The results indicate that the porosity decreases to some extent with the increase of the

mass fractal dimension. For sandy gravel samples, the porosity falls from 0.30 to 0.23, but the mass fractal dimension rises from 2.4767 to 2.7392. Since the mass fractal dimension represents the cumulative characteristic of particles and pores distribution feature, the larger the mass fractal dimension, the more fine particles in the porosity will be filled. When the porosity reaches the minimum value, the pores of soil skeletons are almost fully packed with fine particles, leading to the maximum value of the mass fractal dimension. For coarse sand samples, the porosity drops from 0.25 to 0.18, and the mass fractal dimension rises from 2.7344 to 2.8531. Similarly, for fine sand samples, the porosity decreases from 0.22 to 0.14, but the mass fractal dimension only increases from 2.8759 to 2.9234.

The dry density varies with the mass fractal dimension in soil samples, as shown in Fig. 12. The results show that the dry density increases significantly as the mass fractal dimension grows. For sandy gravel samples, the dry density increases from 1.95 to 2.28, and the mass fractal dimension increases from 2.4767 to 2.7392. The larger the mass fractal dimension, the more finer fractions will be filled in the pores and the greater the dry density. When the mass fractal dimension reaches the magnitude of a certain value, it tends to be low susceptible to the dry density. For coarse sand samples, the dry density increases from 1.73 to 1.85, and the mass fractal dimension rises from 2.7344 to 2.8531. For fine sand samples, however, the dry density increases from 1.52

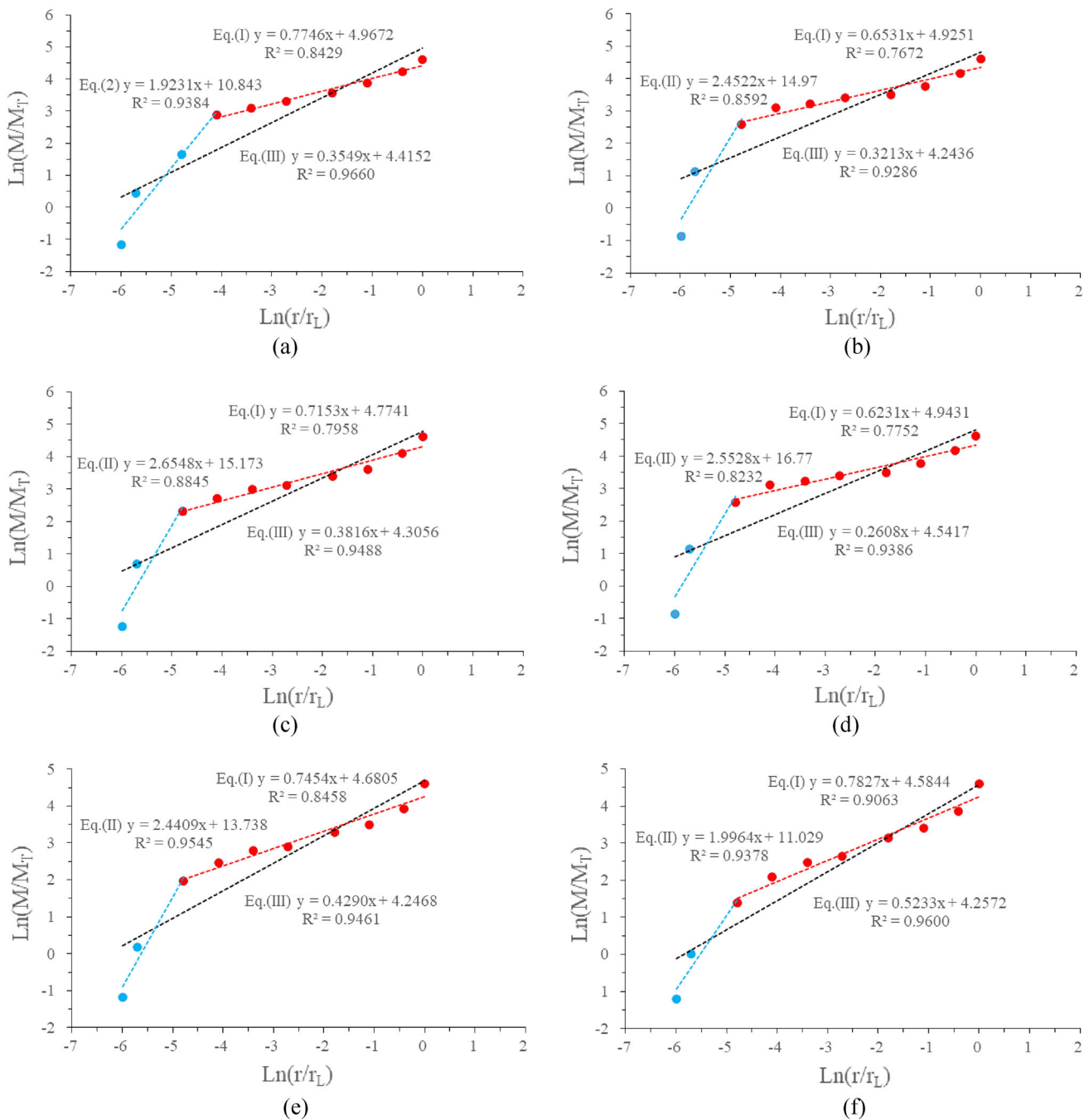


Fig. 6 Fitting results of sandy gravel samples #1–#6. (a–f, respectively)

to 1.72, and the mass fractal dimension only increases from 2.8759 to 2.9234. It is further demonstrated that the mass fractal dimension is closely related to porosity and compactness, which may greatly affect the penetrability of soils.

The permeability coefficient varies with the mass fractal dimension in soil samples, as shown in Fig. 13. There are various factors that affect the permeability coefficient, including grain composition, particle size distribution, soil compactness, grain shape, fluid properties, etc. As discussed above,

the mass fractal dimension is closely related to grain composition, particle size distribution and soil compactness. The results suggest that the permeability coefficient decreases approximately in an exponential form of sandy gravel samples, and in a linear form of coarse sand and fine sand with the increase of the mass fractal dimension. The larger the mass fractal dimension, the more finer fractions will be filled in the pores, the greater the degree of compaction and the more

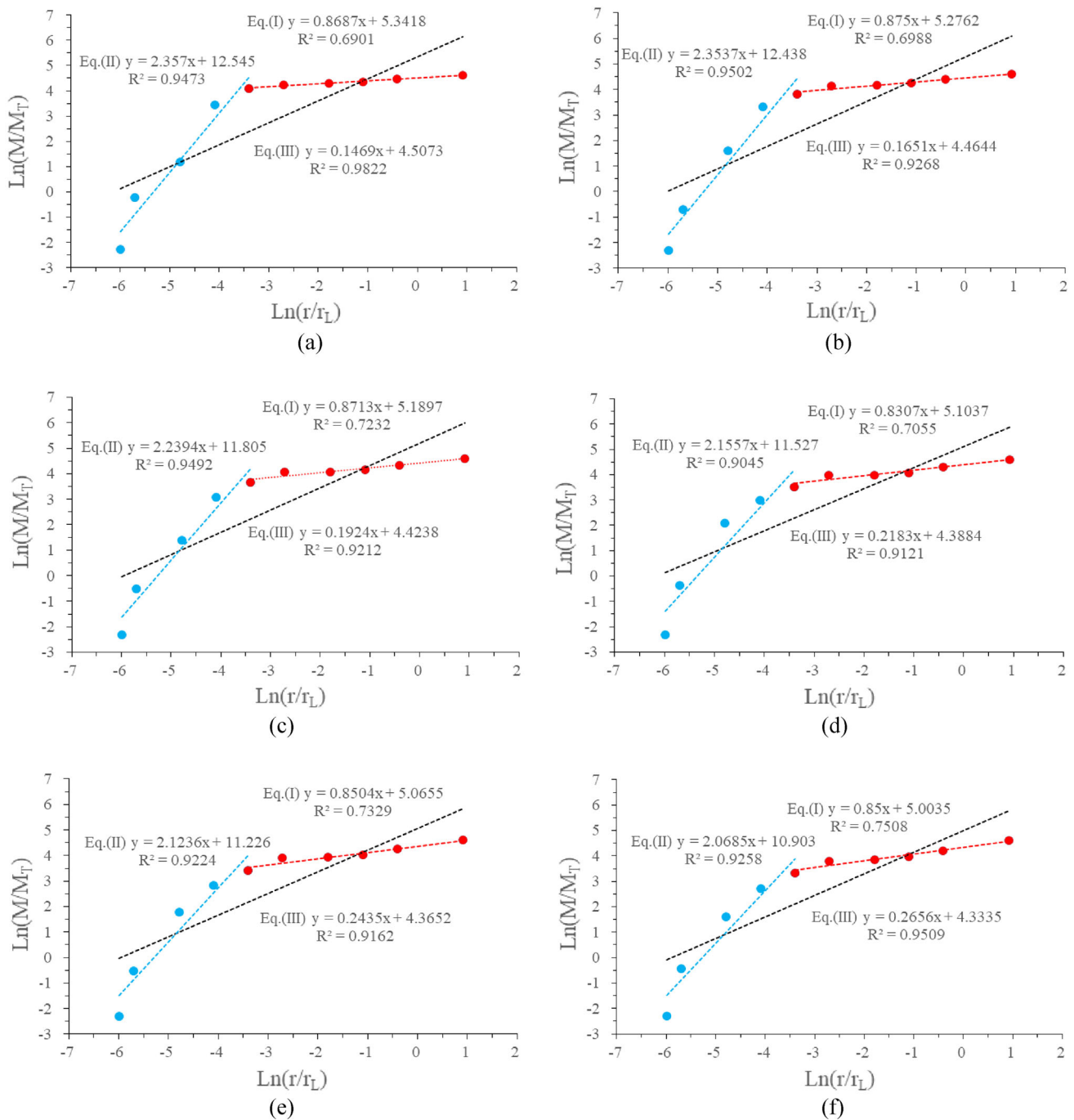


Fig. 7 Fitting results of coarse sand samples #7–#12 (a–f, respectively)

difficult the fluid flows through soil samples. When reaching the magnitude of a certain compaction, the permeability coefficient tends to slowly decline because of the decrease of the connected or effective, pore volume, particularly in coarse sand and fine sand.

3.3 Mass fractal distinction of seepage failure

To better understand the fractal properties in granular soils, a seepage failure type of zone segmentation is proposed by relating the fractal dimension to the critical hydraulic gradient, as shown in Fig. 14. The critical hydraulic gradient here means that the hydraulic gradient reaches a critical state when the seepage force is comparable to the buoyant soil weight per

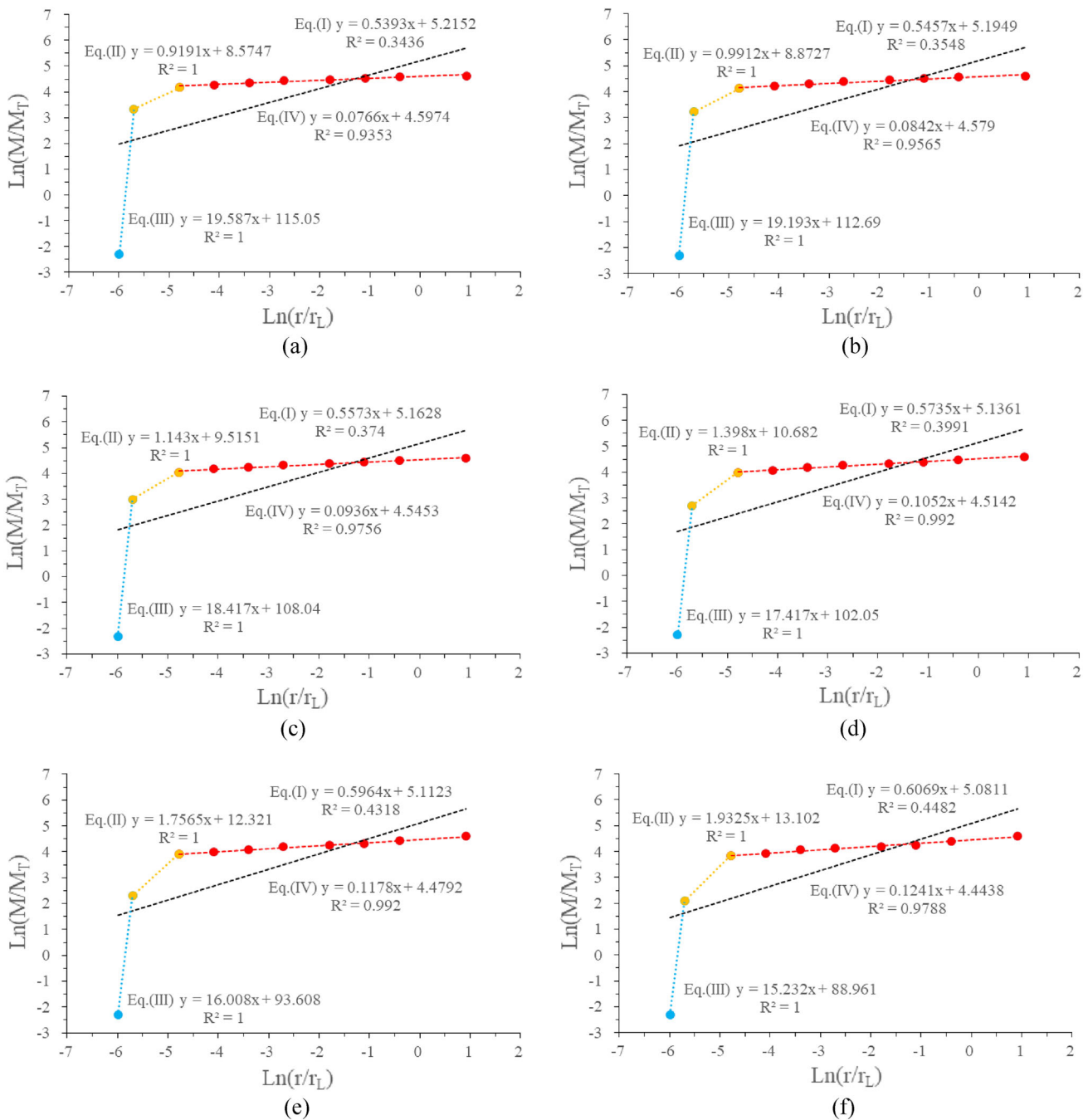


Fig. 8 Fitting results of fine sand samples #13–#18. (a–f, respectively)

unit weight, and soil deformation extends over the entire soil with connected leaky pathways from top to bottom. There is a good agreement between the previous studies and the statistical results obtained from the hydraulic test in this paper [8, 18, 19]. The seepage-induced failure types in granular soils can be divided into three zones: (1) piping that observed in the sandy gravel samples within the critical hydraulic gradient 0.5 and the mass fractal dimension 2.4–2.7, (2) suffosion that observed in the coarse sand samples within the critical

hydraulic gradient 0.4–1.3 and the mass fractal dimension 2.70–2.87, and (3) heave that observed in the fine sand samples within the critical hydraulic gradient 1.0–2.0 and the mass fractal dimension 2.87–3.00.

Sandy gravel samples suffer from piping failure at the critical hydraulic gradient in Zone I, as shown in Fig. 15. At the onset of piping, fine particles were in a state of incipient movement and began to loosen at a small hydraulic gradient, accompanied by observations of a small amount

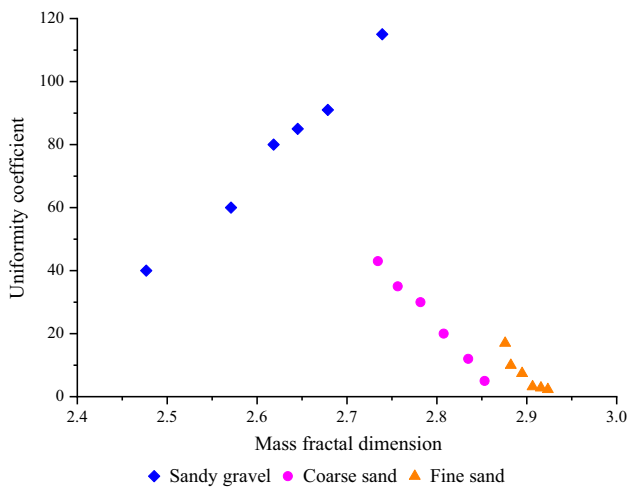


Fig. 9 The relation curves between uniformity coefficient and mass fractal dimension

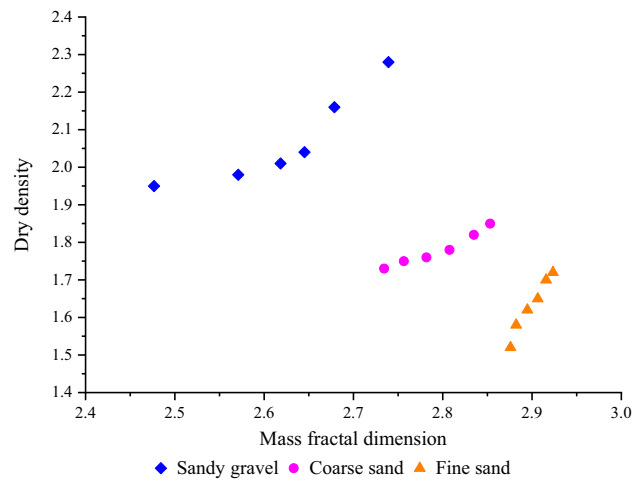


Fig. 12 The relation curves between dry density and mass fractal dimension

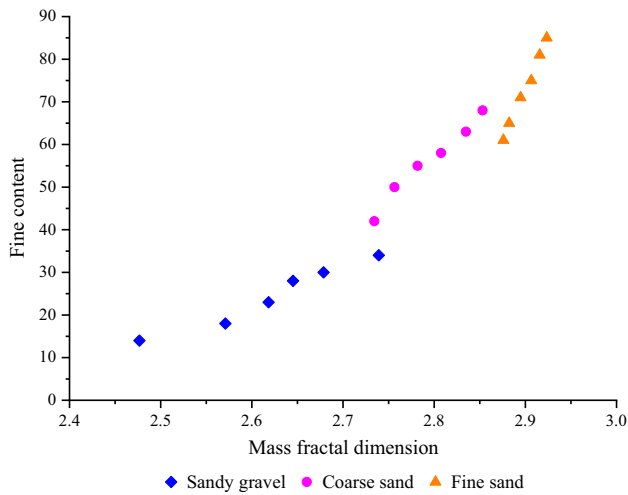


Fig. 10 The relation curves between fine content and mass fractal dimension

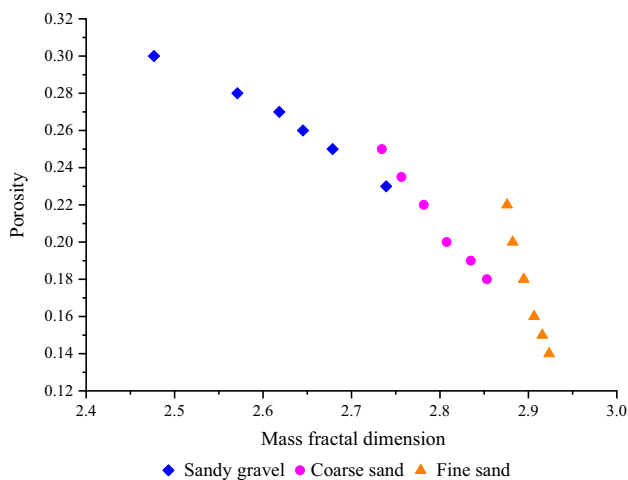


Fig. 11 The relation curves between porosity and mass fractal dimension

of bubbles and outflow water. With the increasing hydraulic gradient, the loose particles began to move, resulting in more void space and larger interstitial voids than before. As the hydraulic gradient increased further, some fine particles were rapidly moved from the pores formed by the steady skeleton and then piled progressively on the surface of soil samples, resulting in the leakage passage affecting the stability of the upper layer. When reaching the magnitude of the critical hydraulic gradient, the washout of finer particles incurs from the concentrated leakage passage through the upstream and downstream, rendering a large amount of turbid overflow water with sand boiling at the exit of the seepage passage.

Piping failure stems from internal instability of nonuniform soils. The uniformity coefficient of sandy gravel samples ranges from 40 to 115, which contains a stable coarser fraction and an erodible finer fraction resided inside the pore spaces of stable skeleton. The piping erosion occurs once the seepage force, caused by the differential heads between the top and bottom of the sample, neutralizes the effective weight and intergrain contact force imposed on the fine particles. As a vertical hydraulic gradient, the seepage force contributes to the migration of fine particles, while the weight and intergrain contact force associated with fine content resists such movement. The higher the fine content, the greater the force at intergrain contacts and the larger the critical hydraulic gradient needed to overcome the seepage resistance. For example, in #6 and #4 sandy gravel samples, the content of fine particles is 14% and 34%, while the critical hydraulic gradient is 0.20 and 0.43, respectively. It is proved to be reasonable that the critical hydraulic gradient increases with the mass fractal dimension related to the uniformity coefficient, porosity and fines content.

External and internal erosion of loose particles lead to suffusion for the coarse sand samples in Zone II, as shown in

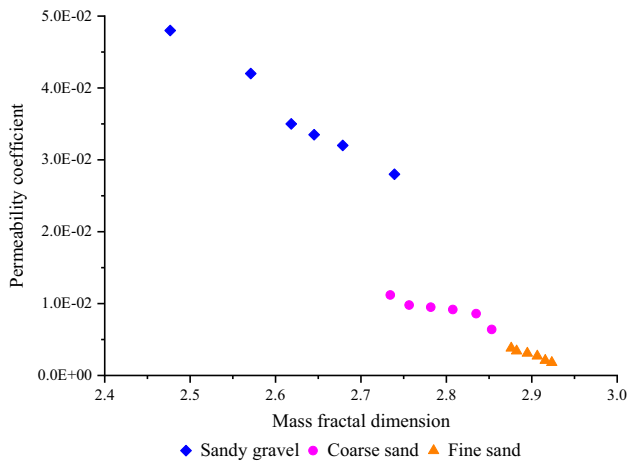


Fig. 13 The relation curves between permeability coefficient and mass fractal dimension

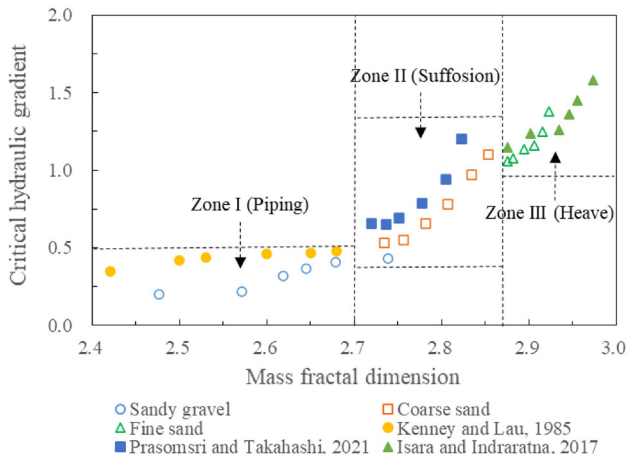


Fig. 14 Statistical results of seepage failure types in different granular soils

Fig. 16. The constant transport of fine particles at a vertical hydraulic gradient from bottom to top results in an increase in the porosity of the underlying soil and the loose grains on the surface of the samples. Over time, these fine particles could be moved left and right to form numerous tiny seepage passages with the increasing hydraulic gradient, accompanied by observations of progressively turbid overflow water and small settlement on the surface of soil samples. The constant washout of fine particles leads to the development and local interconnection of seepage passages through which the fine particles were again moved in groups filling larger pore space. Consequently, suffosion failure eventually appeared either in the external erosion (segregation piping) or in the internal erosion with partial surface collapse due to subsidence deformation.

Compared with the term “suffosion” describing the non-destructive response without changes in volume or mass, the

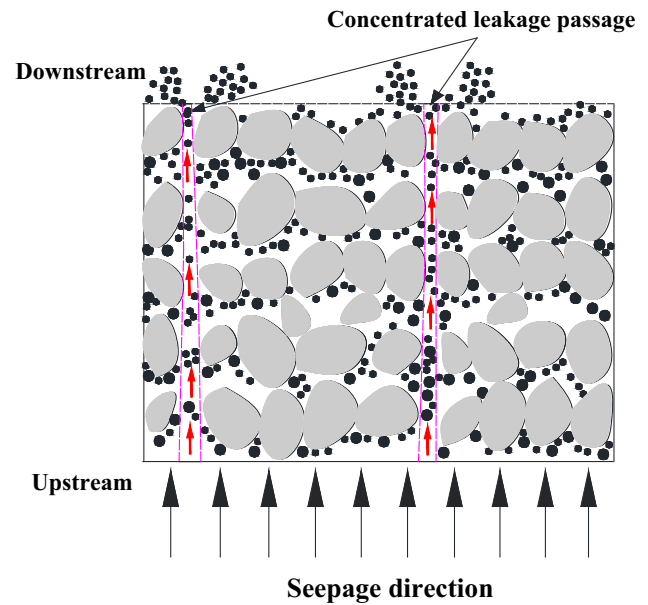


Fig. 15 Illustrations of the mechanism of piping failure in sandy gravels

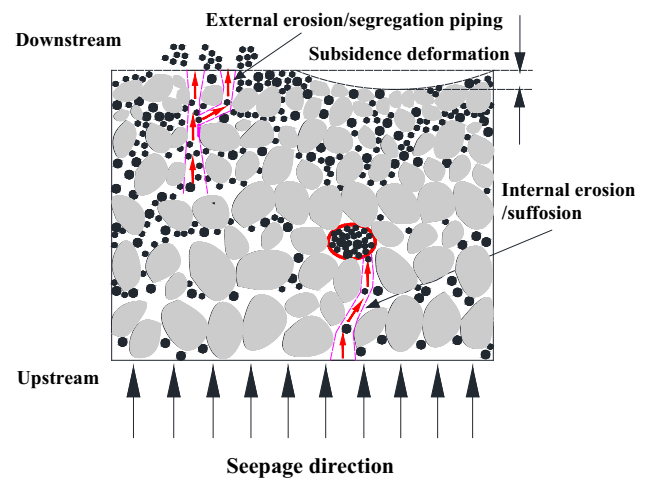


Fig. 16 Illustrations of the mechanism of suffosion failure in coarse sands

term “suffosion” is advocated to describe the instability phenomenon that the fine particles are removed by seepage flow along with a collapse of the soil structure [9]. The occurrence of suffosion failure in the internal part is predominantly governed by the initial fines content, the relative density and the hydraulic gradient [17]. The initial fine content and the relative density are intrinsic factors affecting the stress transfer at intergrain contact of unstable soils, while the hydraulic gradient as an external driving factor promotes the washout of fine particles and the formation of seepage passage. The higher the fine content, the more fine particles participate in stress transfer to the skeleton structure. Once these fine particles are removed by seepage flow in groups, the volumetric strain

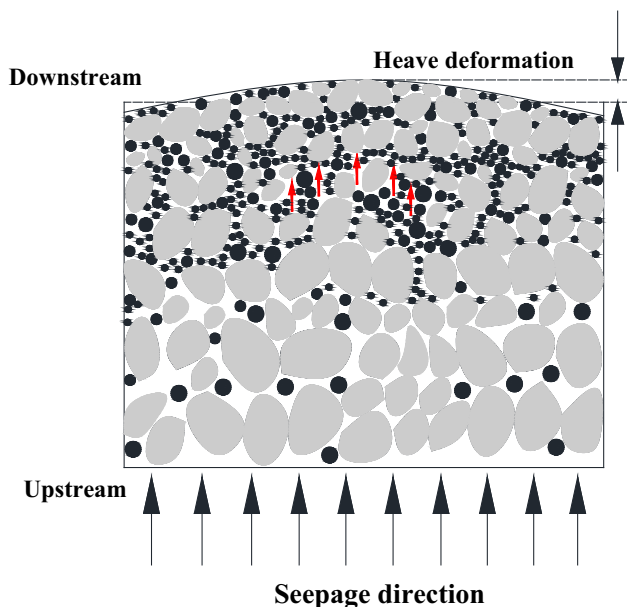


Fig. 17 Illustrations of the mechanism of heave failure in fine sands

is promptly triggered at the critical hydraulic gradient. But if the particles are transported separately by a relatively small seepage flow, the segregation piping may occur in the external erosion. For example, some coarse sandy samples (#10, #11, #12) present the segregation piping, while the others (#7, #8, #9) show the partial surface collapse. As discussed above, the mass fractal dimension is the synthesis of the fine content and the relative density, reflecting the progressive accumulation of fine particles. In addition, it can be deduced that the larger the mass fractal dimension, the greater the critical hydraulic gradient, and the suffoison failure is more likely to occur in coarse sands.

Heave failure occurs in the fine sand samples at the critical hydraulic gradient > 1.0 in Zone III, as shown in Fig. 17. Given the comparatively uniform and compacted particles, most fine particles remained stable even if the hydraulic gradient increased to 0.5, accompanied by various tiny fractures through which a small amount of clean seepage water. As the hydraulic gradient increases, the fine particles constantly move from the underlying position to the upper sample, leading to the packed finer fractions in the upper part, while the accumulated coarser fraction in the underlying part. When reaching the magnitude of the critical hydraulic gradient, the fine particles floated in groups and lifted the coarse particles. As a result, the originally stable structure was completely changed and the surface of the soil sample was progressively heaved.

The onset of the heave failure in the fine sand is subject to the uniformity coefficient (< 20), the fines content ($> 60\%$), the proosity (< 0.22), and the critical hydraulic gradient (> 1.0). Since the mass fractal dimension represents

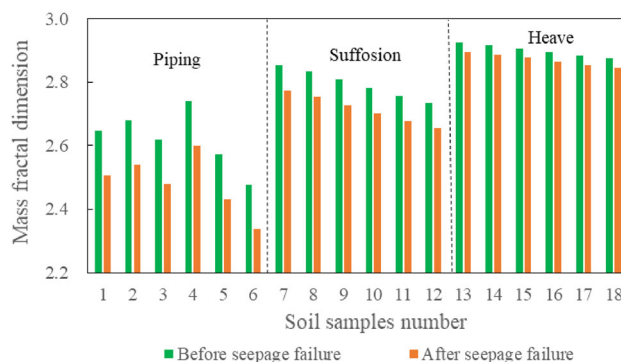


Fig. 18 Mass fractal dimension changes before and after seepage failures in soil samples

the accumulation of particles associated with the uniformity coefficient, the fine content and the porosity, the heave process that the fine particles move from the underlying position to the upper position means the increase of the mass fractal dimension. Therefore, the larger the mass fractal dimension, the greater the resistance imposed by intergrains and surrounding boundaries, and it takes much more seepage force to overcome the resistance. For example, the mass fractal dimension of sample #18 is 2.8759, and the critical hydraulic gradient is 1.06. Comparatively, the mass fractal dimension of sample #13 is 2.9234 with the highest fine content (85%), indicating that the finer fractions were tightly compacted into the pores of the coarser fractions, thus the critical hydraulic gradient rises to 1.38 to break the strong chain of intergrains. As long as the critical hydraulic gradient is large enough to motivate the migration of fine particles in groups, the internal stable fine sand samples are lifted like a rigid soil column with local volume changes. At this time, the seepage and buoyant forces neutralize the effective stresses and boundary friction (resistance), thus allowing the whole soil to move as an entity at the critical hydraulic gradient.

The mass fractal dimension is feasible to distinguish various seepage failures, however, in the process of seepage failure, physico-mechanical parameters (uniformity coefficient, porosity, dry density, permeability coefficient, etc.) change with the transport of fine particles, and the mass fractal dimension changes correspondingly. Given the complex migration of the fine particles, the calculation of the mass fractal dimension is difficult to capture in the seepage process in real time, but the mass fractal dimension changes can be obtained before and after seepage failure in different soil samples, which is important to predict the development of seepage failure, as shown in Fig. 18. The mass fractal dimension before seepage failure may derive from the original grading curves, while the mass fractal dimension after seepage failure can be obtained from the redistributed grading curves due to the sand washed out by overflow water. According to the turbidity of the overflow water and the

characteristics of the gushing sands, the mass fractal dimensions of all the soil samples decrease to different degrees after the seepage failure. For sandy gravel samples, a large amount of turbid water overflows, carrying the sands away at the critical hydraulic gradient. By sieving and measuring the gushing sands, the washout sand size was less than 0.50 mm, and the percentages of these sands (#1–#6) were 18%, 20%, 15%, 22%, 12% and 10%, respectively. Correspondingly, the ratios of the mass fractal dimension fell by 7.5%, 7.8%, 7.3%, 8.2% and 7.1%. For coarse sand samples, the overflow water is little turbid, accompanied by the gushing sand size of less than 0.25 mm, and the percentages of these sands (#7–#12) were 8%, 9%, 7%, 8%, 9% and 8%, respectively. The ratios of the mass fractal dimension were accordingly reduced by 4.5%, 4.3%, 4.5%, 4.3%, 4.5% and 4.6%. Comparatively, the overflow water through the fine sand samples was small and slightly turbid, with the observation of less than 0.10 mm gushing sand size at the large hydraulic gradient. The percentages of the gushing sands (#13–#18) were 5%, 4%, 3%, 4%, 5% and 4%, and the ratios of the mass fractal dimension fell 1.8%, 1.9%, 2.2%, 2.3%, 2.2% and 2.4%, respectively.

As discussed above, the mass fractal dimension represents the accumulation characteristics of soil particles, integratively reflecting the fine content, the uniformity coefficient, the porosity and the permeability. In the process of piping failure in sandy gravel, the exit of the leakage passage releases the concentrated stress of the fine particles, so the mass fractal dimension obviously decreases with the amount of gushing fines. Similarly, in the process of suffosion failure in coarse sand, particularly in the external erosion of segregation piping, the exit of numerous tiny seepage passages partially reduced the concentration of stress, resulting in a decrease in the mass fractal dimension along with the gushing fine particles. However, in the process of heave failure in fine sand, the vast majority of fine particles filled the porosity of the upper layer by the large vertical hydraulic gradient, leaving a tiny amount of fine particles floating on the surface of the soil samples. At this time, concentrated stress may not be released without any leakage passages. Consequently, with a small amount of fine particles, the mass fractal dimension hardly declined. In short, it is feasible to predict the seepage failure in sandy gravels and coarse sands by comparing the mass fractal dimension, while it is nearly impossible to predict heave failure in the fine sands.

4 Conclusions

In this study, a series of hydraulic tests were conducted to show the fractal characteristics of seepage-induced failure in granular soil. The main conclusions are as follows:

- (1) The mass fractal dimension is appropriate to describe the cumulative mass distribution of particles, which governs most of the physical properties of granular soils. The accurate calculation of the scale-invariant interval is the precondition for determining the mass fractal dimension. The scale-invariant intervals of sandy gravel range from 1 to 20 mm, while coarse sands range from 0.5 to 10 mm and fine sands from 0.25 to 5 mm. The fine content of the scale-invariant interval largely determines the magnitude of the mass fractal dimension, and the higher the fine content of the scale-invariant interval, the larger the mass fractal dimension.
- (2) The mass fractal dimension is closely related to the uniformity coefficient, fine content, porosity, dry density and permeability coefficient. The uniformity coefficient increases with the mass fractal dimension, while the nonuniformity of granular soil is greatly reduced when fine particles progressively accumulate to a certain degree. The increase of the mass fractal dimension indicates that more fine particles fill the pore networks, resulting in an increase in fine content and dry density but a decrease in porosity and permeability coefficient. When the mass fractal dimension reaches the larger magnitude, the permeability coefficient in fine sand tends to slowly decline because of the decrease in the effective pore volume.
- (3) By linking the mass fractal dimension and the critical hydraulic gradient, the seepage-induced failure type in granular soils can be divided into three zones: (i) piping of sandy gravels within the critical hydraulic gradient 0.5 and the mass fractal dimension 2.4–2.7, (ii) suffosion of coarse sands within the critical hydraulic gradient 0.4–1.3 and the mass fractal dimension 2.70–2.87, and (iii) heave of fine sands within the critical hydraulic gradient 1.0–2.0 and the mass fractal dimension 2.87–3.00. It is feasible to predict the piping in sandy gravels and suffosion in loose coarse sands by comparing the changes of the mass fractal dimension before and after seepage failure, while it is almost impossible to predict heave failure in fine sands.

Fractal analysis of hydraulic tests provides a new understanding of the particle mechanics of the seepage-induced failures in granular soil. The results may be of interest to hydrologists and geotechnical engineers concerned with groundwater. This paper is limited to three types of granular soils by statistical results of the hydraulic tests. Further research with a wider variety of soil types and more advanced visualization technology is encouraged to provide a deeper understanding of the mechanisms of the seepage failure.

Acknowledgements This work was supported by the General Project of Philosophy and Social Science Research in Jiangsu Universities (2022SJYB0841).

Declarations

Conflict of interest The authors declare that there is no conflict of interest in this paper.

References

- Fukumoto Y, Yang H, Hosoyamada T, Ohtsuka S (2021) 2-D coupled fluid-particle numerical analysis of seepage failure of saturated granular soils around an embedded sheet pile with no macroscopic assumptions. *Comput Geotech* 136:104234
- Wörman A, Olafsdottir R (2010) Erosion in a granular medium interface. *J Hydraul Res* 30:639–655
- Bendahmane F, Marot D, Alexis A (2008) Experimental parametric study of suffusion and backward erosion. *J Geotech Geoenviron Eng* 134:57–67
- Richards KS, Reddy KR (2012) Experimental investigation of initiation of backward erosion piping in soils. *Geotechnique* 62:933–942
- Tian KL, Yang AQ, Nie KY, Zhang HL, Xu J, Wang XD (2020) Experimental study of steady seepage in unsaturated loess soil. *Acta Geotech* 15:2681–2689
- Luo YL, Jin X, Li X, Zhan ML, Sheng JC (2013) A new apparatus for evaluation of contact erosion at the soil-structure interface. *Geotech Test J* 36:256–263
- Ke L, Takahashi A (2014) Experimental investigations on suffusion characteristics and its mechanical consequences on saturated cohesionless soil. *Soils Found* 54:713–730
- Prasomsri J, Takahashi A (2021) Experimental study on suffusion under multiple seepages and its impact on undrained mechanical responses of gap-graded soil. *Soils Found* 61:1660–1680
- Hunter RP, Bowman ET (2017) Visualisation of seepage induced suffusion and suffusion within internally erodible granular media. *Geotechnique* 68:1–48
- Zhong C, Le VT, Bendahmane F, Marot D, Yin ZY (2018) Investigation of spatial scale effects on suffusion susceptibility. *J Geotech Geoenviron Eng* 144:04018067
- Gu DM, Huang D, Liu HL, Zhang WG, Gao XC (2019) A DEM-based approach for modeling the evolution process of seepage-induced erosion in clayey sand. *Acta Geotech* 14:1629–1641
- Yang J, Yin ZY, Laouafa F, Hicher PY (2020) Hydromechanical modeling of granular soils considering internal erosion. *Can Geotech J* 57:157–172
- Chapuis RP (1992) Similarity of internal stability criteria for granular soils. *Can Geotech J* 29:711–713
- Bi JF, Zhang HT, Luo XQ, Shen H, Li ZM (2021) Modeling of internal erosion using particle size as an extra dimension. *Comput Geotech* 133:1–14
- Qian JG, Li WY, Yin ZY, Yang Y (2021) Influences of buried depth and grain size distribution on seepage erosion in granular soils around tunnel by coupled CFD-DEM approach. *Transp Geotech* 29:100574
- Chang DS, Zhang LM (2013) Extended internal stability criteria for soils under seepage. *Soils Found* 53:569–583
- Slangen P, Fannin RJ (2017) A flexible wall permeameter for investigating suffusion and suffosion. *Geotech Test J* 40:1–14
- Kenney TC, Lau D (1985) Internal stability of granular filters. *Can Geotech J* 22:215–225
- Israr J, Indraratna B (2017) Internal stability of granular filters under static and cyclic loading. *J Geotech Geoenviron Eng* 143:1–16
- Turcotte DL (1997) *Fractals and chaos in geology and geophysics*. Cambridge University Press, New York
- Yu BM, Cheng P (2002) A fractal permeability model for bi-dispersed porous media. *Int J Heat Mass Transf* 45:2983–2993
- Yu BM (2008) Analysis of flow in fractal porous media. *Appl Mech Rev* 61:050801
- Wu MY, Liu JJ, Lv XF, Shi D, Zhu ZW (2018) A study on homogenization equations of fractal porous media. *J Geophys Eng* 15:2388–2398
- Tyler SW, Wheatcraft SW (1992) Fractal scaling of soil particle-size distributions: analysis and limitations. *Soil Sci Soc Am J* 56:362–369
- Wang M, Yang W, Zhou Z, Yang J, Yang F, Sheng S (2022) Experimental study on fractal characteristics of fault filling medium in the tunnel and relationship between fractal dimension and permeability coefficient. *Geomech Geophys Geo-energy Geo-resour* 8:6
- Li B, Liu R, Jiang Y (2016) A multiple fractal model for estimating permeability of dual-porosity media. *J Hydrol* 540:659–669
- Shepard JS (1993) Using a fractal model to compute the hydraulic conductivity function. *Soil Sci Soc Am J* 57:300–306

Publisher's Note Springer Nature remains neutral with regard to jurisdictional claims in published maps and institutional affiliations.

Springer Nature or its licensor (e.g. a society or other partner) holds exclusive rights to this article under a publishing agreement with the author(s) or other rightsholder(s); author self-archiving of the accepted manuscript version of this article is solely governed by the terms of such publishing agreement and applicable law.